The role of ARF1 in unconventional secretion of transmembrane protein

Soo Kyung Seo

Department of Medical Science
The Graduate School, Yonsei University

The role of ARF1 in unconventional secretion of transmembrane protein

Directed by Professor Min Goo Lee

The Doctoral Dissertation
submitted to the Department of Medical Science,
the Graduate School of Yonsei University
in partial fulfillment of the requirements for the degree of
Doctor of Philosophy in Medical Science

Soo Kyung Seo

December 2022

This certifies that the Doctoral Dissertation of
Soo Kyung Seo is approved.

Thesis Supervisor : Min Goo Lee

Thesis Committee Member #1 : Heon Yung Gee

Thesis Committee Member #2 : Seung-Yeol Park

Thesis Committee Member #3 : Jae Myun Lee

Thesis Committee Member #4 : Jeon-Soo Shin

The Graduate School
Yonsei University

December 2022

ACKNOWLEDGEMENTS

길다면 길고 짧다면 짧은 학위 과정의 끝이 다가오네요. 끝나는 날이 올 줄 몰랐는데, 그 순간을 갑자기 맞이 하는 것 같아 아직 실감이 잘 나지 않습니다. 많이 부족하였고, 많은 경험을 하였고, 많이 배웠습니다. 앞으로도 실험실에서 배운 내용을 바탕으로 연구에 정진하여 어디에서도 부끄럽지 않은 사람이 되겠습니다. 학위 과정 동안 많이 부족한 모습에도 기다리고 믿고 맡겨주신 이민구 교수님께 감사의 말씀 올립니다.

학위 기간 동안 많은 것을 알려주시고 좋은 말씀 많이 해주신 김연정 선생님, 노신혜 선생님, 신동훈 선생님, 송민석 선생님과 지도교수가 아님에도 관심을 가지고 지켜봐 주신 지헌영 교수님, 김한상 교수님께도 감사인사를 전하고 싶습니다. 같이 동고동락 했던 유정우 선생님, 심주리 선생님, 민재, 은성호 선생님, 이영채 선생님, 박해니 선생님, 엄소원 선생님, 신선미 선생님과 실험적으로나 정신적으로 많은 도움을 준 영익 오빠, 세영쌤, 선영이에게 고맙다는 말 전하고 싶습니다. 여러 상황에서 도움과 위로를 많이 해준 예진이, 실험실 생활에 큰 의지가 된 동건이 에게도 고맙다는 인사 전하고 싶습니다. 운 좋게 좋은 실험실 선생님들을 만나 큰 걱정 없이 무탈하게 마무리 할 수 있었습니다. 다들 감사 드리고 모두 열심히 하시는 만큼 좋은 결실 맺으시길 바라겠습니다.

마지막으로, 학위 기간 동안 많은 지지를 해준 엄마, 아빠와 삶의 활력소가 되었던 언니, 유정이, 형부 그리고 원우에게 감사의 마음을 전합니다.

2022.12

<TABLE OF CONTENTS>

LIST OF FIGURES

ABSTRACT

The role of ARF1 in
unconventional secretion of transmembrane protein

Soo Kyung Seo

Department of Medical Science
The Graduate School, Yonsei University

(Directed by Professor Min Goo Lee)

The majority of transmembrane proteins are conventionally transported through the endoplasmic reticulum (ER) to the Golgi apparatus and then to the plasma membrane. However, studies have shown that some proteins can reach the plasma membrane via an alternative route known as the unconventional protein secretion (UPS) pathway. Despite ongoing research, the underlying molecular mechanism of UPS has yet to be elucidated. This study reveals that the UPS of transmembrane protein requires ARF1 activation. An ARF1-GTP-restricted mutant powerfully rescues cystic fibrosis transmembrane conductance regulator (CFTR) and full-length Spike (S) protein on the plasma membrane. Conversely, gene silencing of ARF1 blocks unconventional trafficking of CFTR and S protein. Activated ARF1 interacts with OSBPL1 and VAPA, forming an ARF1-OSBPL1-VAPA complex that induces autophagosome formation near CFTR trapped in the ER. These results suggest that ARF1 plays a key role in Golgi-bypassing trafficking of transmembrane proteins.

Key words : ARF1; unconventional protein secretion; CFTR; Spike; SARS-CoV-2; ORF3a; VAPA; OSBPL1; autophagosome

The Role of ARF1 in Unconventional Secretion of Transmembrane Protein

Soo Kyung Seo

Department of Medical Science
The Graduate School, Yonsei University

(Directed by Professor Min Goo Lee)

I. INTRODUCTION

In eukaryotic cells, most transmembrane proteins synthesized in the endoplasmic reticulum (ER) are subsequently transferred to the Golgi apparatus in a process called conventional trafficking. However, recent studies have shown that some proteins are also secreted through unconventional protein secretion (UPS) that bypasses the Golgi apparatus during stress conditions.[1,2] Research indicates that UPS is related to Golgi reassembly-stacking proteins of 55 kDa (GRASP55)[3] and autophagosome formation[4] and is triggered by inositol-requiring enzyme 1α (IRE1α) among several other ER stress signals.[5] However, The underlying mechanism of UPS remains unclear.

Cystic fibrosis conductance regulator (CFTR) is a transmembrane protein that transports anions such as Cl^- and $HCO3^-$ across the apical membrane.[6] A genetic variant of CFTR, which has a deletion of the 508th phenylalanine known as ΔF508-CFTR, is the most prevalent cause of cystic fibrosis.[7] Due to its folding defect, this genetic variation is retained in the ER rather than transferring to the plasma membrane.[8] Recent studies have shown that CFTR can transfer to the cell membrane via UPS.[3] CFTR is an N-glycosylated protein. Under normal conditions, surface expression of CFTR appears in the form of complex glycosylated CFTR, which travels through conventional protein secretion.[7] Under ER stress, however, CFTR detected in the plasma membrane has a core-glycosylated form because it

bypasses the Golgi apparatus.[3]

Severe acute respiratory syndrome coronavirus 2 (SARS-CoV-2) is the virus responsible for the COVID-19 pandemic. The Spike (S) protein, the viral envelop protein of SARS-CoV-2, binds to angiotensin-converting enzyme 2 (ACE2) receptors and is cleaved by transmembrane serine protease 2 (TMPRSS2) on the host cell surface to fuse with the host cell membrane.[9] There is a furin cleavage site between S1 and S2 fragments of the S protein so that it can be cleaved by endogenous furin in the host cells.[10] Thus, both full-length S and cleaved S poteins can be observed in cell lysates. S proteins are synthesized in the ER and transported to the plasma membrane and double-membrane vesicles where the virus assembles.[11] The underlying mechanism remains unclear.

ADP-ribosylation factor1 (ARF1) is a small guanine nucleotide-binding protein with GTPase activity. ARF1 changes its conformation depending on the GTP or GDP combination.[12] This property gives ARF1 the ability to anchor the membrane and play a role in recruiting coat protein complexes and the formation of membrane contact sites (MCS).[13,14] Previous studies have shown that mutation of ARF1 induces UPS.[3-5,15] Notably, ARF1-Q71L-induced ER-to-Golgi blockade results in powerful UPS over a short period, although the level of ER stress is considerably lower than in other methods. As a result, we hypothesized that ARF1 mediates UPS of transmembrane protein.

In this study, we used two dominant-negative mutants of ARF1 to investigate this mechanism. The first one is ARF1-Q71L, a GTP-bound ARF1 mutant that blocks retrograde transport.[16,17] Overexpression of this mutant accumulates proteins in the ER-Golgi intermediate compartment (ERGIC) and Golgi apparatus.[16] The second mutant is ARF1-T31N, a GDP-bound mutant that inhibits anterograde transport and accumulation of proteins in ER.[16] This study demonstrated that ARF1-GTP mediates UPS of CFTR and SARS-CoV-2 S protein. This newly identified mechanism provides insight into the UPS pathway and potential treatment strategies for human diseases caused by defects in protein secretion.

II. MATERIALS AND METHODS

1. Plasmid cloning and siRNA transfection

Plasmids expressing pCMV-ΔF508-CFTR, pClneo-HA-STX5, pClneo-SAR1-T39N-MYC, and pcDNA3.1-Spike have been described previously.[3,15] pCMV6-VAPA-MYC-FLAG (Origene #RC201164, Rockville, MD, USA) and pCMV6-VAPB-MYC-FLAG (Origene #194434, #RC200517, Rockville, MD, USA) plasmids were commercially purchased. The pcDNA3-ARF1-Q71L-HA and pcDNA3-ARF1-T31N-HA plasmids were commercially custom-synthesized and cloned into a pcDNA3 vector. pcDNA3-ORF3a-HA plasmids were cloned from the cDNA of SARS-CoV-2 genomic RNA using the PCR-based Gibson assembly method (New England BioLabs® Inc #E2621L, Ipswich, MA, USA).

ON-TARGETplus human ARF1-specific, AP1G1-specific, AP3D1-specific, AP4E1-specific, COPB1-specific, VAPA-specific, VAPB-specific, TMED-specific, GRASP55-specific, and control scrambled siRNAs were commercially purchased (SMARTpool siRNAs: ARF1, gene ID 375; AP1G1, gene ID 164; AP3D1, gene ID 8943; AP4E1, gene ID 23431; COPB1, gene ID 1315; VAPA, gene ID 9218; VAPB, gene ID 9217; TMED2, gene ID 10959; TMED3, gene ID 23423; TMED9, gene ID 54732; TMED10, gene ID 10972; GORASP2, gene ID 26003, Lafayette, CO, USA).

The transfection of plasmids was performed with lipofectamine LTX reagent (Invitrogen #15338500, Waltham, MA, USA) and siRNAs were transfected with Lipofectamine RNAimax transfection reagent (Invitrogen #13778100). Both transfections were conducted according to the manufacturer′s protocol.

2. Chemical reagents and antibodies

Thapsigargin and ponceau S were purchased commercially, and (E)-2-(2-chlorostyryl)-3,5,6-trimethyl-pyrazine (CSTMP) was synthesized commercially (Cayman Chemical #1000672-89-8, Ann Arbor, MI, USA). The following antibodies were acquired commercially: anti-CFTR (Millipore #05-583, Billerica, MA, USA;

Alomone Labs #ACL006, Jerusalem, Israel), anti-ARF1 (Abcam #183576, Cambridge, UK), anti-HA (Cell Signaling Technology #2367, Danvers, MA, USA), anti-Myc (Cell Signaling Technology #2276), anti-DYK (Cell Signaling Technology #2368), anti-Aldolase A (Santa Cruz #sc-390733, Dallas, TX, USA), anti-GM130 (BD Biosciences #610899, Franklin Lakes, NJ, USA), anti-Calnexin (Abcam #ab219644), anti-IRE1α (Cell Signaling Technology #3294), anti-phospho S724 IRE1α (Abcam #ab48187), anti-LC3 (Sigma-Aldrich #4108S, St. Louis, MO, USA), anti-Furin (Invitrogen #PA1-062), anti-GRASP55 (Abcam #ab74579), anti-SARS-CoV-2 S1 (GeneTex #GTX135356, Irvine, CA, USA), and anti-SARS-CoV-2 S2 (GeneTex # GTX632604).

3. Surface biotinylation and immunoblotting

HEK293 cells were grown on 6-well plates rinsed with poly-D-lysine. Then, 48 hours after transfection, the cells were washed three times with ice-cold phosphate-buffered saline (PBS). The surface proteins of the cells were biotinylated with Sulfo-NHS-SS-Biotin (Thermo Pierce #21331, Waltham, MA, USA) in chilled PBS for 30 minutes on ice in the dark. After the reaction, quenching was performed with 1% bovine serum albumin (BSA) in PBS for 5 minutes. Next, the BSA solution was washed out with ice-cold PBS. The cells were lysed with lysis buffer [20 mM Tris (pH 7.4), 150 mM NaCl, 1% (v:v) NP40, 0.5% (v:v) sodium deoxycholate, 10% glycerol, 1 mM EDTA, and protease inhibitor cocktail (Roche #04693159001)] and centrifuged at 13,200 rpm for 20 minutes at 4℃. The cells were lysed with RIPA buffer [50 mM Tris (pH 7.4), 150 mM NaCl, 1% (v/v) NP40, 0.5% (v:v), sodium deoxycholate, 2 mM MgCl2, 2 mM EDTA, 1% (v:v) sodium dodecyl sulfate, 1 mM EDTA, and protease inhibitor cocktail] to analyze LC3 proteins, which are difficult to detect due to its lipidation. After centrifugation, only supernatant was collected, and the protein concentration was quantified using a Bradford assay (Bio-RAD #5000006, Hercules, CA, USA). Next, 400 μg of protein from each sample was agitated overnight at 4℃ with 300 μL 5% streptavidin agarose (Thermo Pierce #20349). The biotinylated protein bound to the agarose was eluted using 2X SDS

sample buffer with 0.02 g/ml DL-dithiothreitol (DTT, Sigma-Aldrich #43815) at 37℃ for 30 minutes. The whole-cell lysate and eluted biotinylated samples were then loaded onto SDS-polyacrylamide gel (SDS-PAGE, KOMA BIOTECH #KG50105; #KG70705, Seoul, Korea), separated by gel electrophoresis, and transferred to a nitrocellulose membrane (Amersham #10600004, Chicago, IL, USA). The membrane was incubated in a blocking solution containing 5% skim milk in TBS-T for 30 minutes and blotted with the appropriate primary and HRP-conjugated secondary antibodies. The blots were observed using enhanced chemiluminescence detection reagent (ECL, Amersham #RPN2134).

4. RNA extraction and RT-qPCR

RNA extraction from the cells was performed with AccuPrep Universal RNA Extraction Kit (Bioneer #K-3140, Daejeon, Korea) 48 hours after transfection with siRNA according to the manufacturer′s protocol. For reverse transcription from RNA to cDNA, 1 μg of total RNA was mixed with RNA to cDNA EcoDry Premix (Takara #639549, San Jose, CA, USA) and incubated at 42˚C for 1 hour. To stop the reaction, the sample was incubated at 70˚C for 10 minutes.

The primer sequences used for the qPCR analysis were the following : GAPDH, forward primer 5′-AAT CCC ATC ACC ATC TTC CA-3′, reverse primer 5′-TGG ACT CCA CGA CGT ACT CA-3′; AP1G1, forward primer 5′-CTC TGT GAC ACG AGG TTA TGC C-3′, reverse primer 5′-CTG CTG GAG TTC CAC ATC AAT GC-3′; AP3D1, forward primer 5′-TCG TCA CAG AGG AGA TGC CTG-3′, reverse primer 5′-GCA GTT TCT CGC TGT CGG CTA A-3′; AP4E1, forward primer 5′-CAT CAA CGC CAG GAG GAA AAG C-3′, reverse primer 5′-GAA ATG CCA GCA GGA GAC TGT C-3′; COPB1, forward primer 5′-GCA ACT CAG AGT GCC CTT AGC A-3′, reverse primer 5′-GCA ATC TTG GTC AGA GTT GTG GC-3′; OSBP, forward primer 5′-CTG GAC CGA TTA GAG GAG AAT GG-3′, reverse primer 5′-TTT CCT GAC GCA ATG TCC

AGC C-3′; OSBP2, forward primer 5′-CAG CCT TAA CCT CTG GAG CAT C-3′, reverse primer 5′-TGG TAC TCC AGG TCC TCT GTC A-3′; OSBPL1, forward primer 5′-AGA GCA GTC TCT GGT GAA AGG C-3′, reverse primer 5′-TCA AAG GAG CGT GCT GTC ACT G-3′; OSBPL3, forward primer 5′-GTG GAA AAG CGG TTC ATC GGC T-3′, reverse primer 5′-CTC GTA GCC TTT CGG CAT AGG A-3′; OSBPL6, forward primer 5′-CAC CTC ACT GAC CCT CTG GAA A-3′, reverse primer 5′-CTC GGA AAC CAT CTG CTT CAG C-3′; OSBPL7, forward primer 5′-CAC ACG GAG TTC TTC GAT GCC T-3′, reverse primer 5′-AGG TCC AGC ATC TCC TCA GAC A-3′; OSBPL9, forward primer 5′-AGT CAG AGC AGC GTC CAT CTT C-3′, reverse primer 5′-AGT GAG ACT GCT ACT CGG TGG T-3′; TMED2, forward primer 5′-GCT GTA AAG CAC GAA CAG GA-3′, reverse primer 5′-AGG ACC AAA GGA CCA CTC TG-3′; TMED3, forward primer 5′-TGA TTG ACT CCC AGA CGC AT-3′, reverse primer 5′-GAC TGA AGC TGA CCA CGA AC-3′; TMED9, forward primer 5′-TGC GAC CGA TGA CTA TGA CA-3′, reverse primer 5′-GAG CCT CTC TCC ACA TCT CC-3′; and TMED10, forward primer 5′-CCT GAC CAA CTC GTG ATC CT-3′, reverse primer 5′-CGT TGG TAT CAC GCA TCT CC-3′.

5. Immunoprecipitation and semi-pull-down assay

For immunoprecipitation, HEK293 cells were grown on 6-well plates rinsed with poly-D-lysine. Then, 48 hours after transfection, the cells were washed three times with ice-cold PBS. The cells were lysed with lysis buffer [20 mM Tris (pH 7.4), 150 mM NaCl, 1% (v:v) NP40, 10% glycerol, 1 mM EDTA, and protease inhibitor cocktail] and centrifuged at 13,200 rpm for 20 minutes at 4℃. After centrifugation, the supernatant was collected, and the protein concentration was quantified using a Bradford assay. Next, 400 μg of protein from each sample was agitated at 4℃ overnight with 300 μl 5% A/G beads bound with the appropriate antibodies. The proteins bound to agarose were eluted

using 2X SDS sample buffer, separated by SDS-PAGE, transferred, and immunoblotted as previously described.

A semi-pull-down assay was performed with GGA3 as a bait that binds the bound form of ARF1-GTP only. HEK293 cells were washed with ice-cold PBS and lysed with lysis buffer with phosphatase inhibitor. The commercial ARF1 activation assay kit (MyBioSource #MBS168564, San Diego, CA, USA) was used in accordance with the manufacturer′s protocol.

6. Immunofluorescence

HeLa cells were first grown on an 18-mm coverslip. Then, 24 hours after transfection, the cells were fixed with 4% paraformaldehyde for 10 minutes, permeabilized with 1% Triton X-100 in PBS for 10 minutes, and washed twice with PBS. They were then incubated with a blocking solution containing 2% bovine serum albumin (BSA) at room temperature for 30 minutes. The cells were incubated with the appropriate primary antibodies at 4˚C overnight, washed with PBS and stained with a secondary antibody conjugated with fluorochrome at room temperature for 30 minutes. Then, the cells were washed with PBS, mounted to glass slides using a mounting solution (Agilent Dako #S3025, Santa Clara, CA, USA), and observed with a confocal fluorescent microscope (LSM 980; Carl Zeiss, Berlin, Germany) with a 63× 1.4 numerical aperture oil objective lens.

7. Virus propagation, quantifications, and infection of SARS-CoV-2

A clinically isolated SARS-CoV-2 KUMC-2 strain (GISAID accession #EPI_ISL_413018) was provided by Prof. MS Park at Korea University. To propagate the viruses, Vero cells were infected by SARS-CoV-2 with 0.01 multiplicity of infection (MOI), and then the culture supernatant was harvested at 24-48 hr post-infection. The harvested supernatant was filtered and stored at -80℃.

For viral infection assays, target cells were incubated with virus of 0.01 MOI for 1 hr

and then replaced with 2% FBS medium until a subsequent experiment. To obtain lentiviral particles, pLKO.1 shRNA plasmids (1 μg) were co-transfected with psPAX2 packaging plasmids (750 ng) and pMD2.G envelope plasmids (250 ng) into HEK293T cells. To establish stable TMED knockdown cell lines, Vero cells were infected with lentiviral particles purified from supernatants of HEK293T cells expressing TMED3, TMED9, TMED10, and TMED2 shRNAs. After 24 hr, the supernatant was replaced with a complete medium supplemented with 5 μg/mL puromycin. Puromycin selection was then conducted, and the transduced cells were harvested for qPCR analysis. The target sequences of shRNAs were the following: TMED2 (gene ID: 10959) 5′- GAG CCA TCA ACG ACA ACA CAA-3, TMED3 (gene ID: 23423) 5′- CTC TCA CAA GAC CGT CTA CTT -3′, TMED9 (gene ID: 54732) 5′- GCT GCT AAA GAC AAG TTG AGT -3′, and TMED10 (gene ID: 10972) 5′- CAA CAA ACA CTC GGG TCC TAT -3′. All of the experiments with infectious viruses were approved by the Institutional Biosafety Committee of Yonsei University Health System (IBC 2020-003) and conducted in the Biosafety Level 3 facility at Yonsei University College of Medicine.

8. Quantifications of viruses

To quantify the SARS-CoV-2 virus secretion, viral RNA in cell culture supernatant was extracted using a QIAamp Viral RNA Mini kit (QIAGEN #52906, Valencia, CA, USA), as per the manufacturer's instructions. Quantitative PCR was performed with a Luna® Universal One-Step RT-qPCR Kit (New England BioLabs® Inc) using the ABI Prism 7000 detection system (Applied Biosystems, Waltham, MA, USA). For amplification, 2 μL of extracted RNA was added to a mixture of 10 μL of 2X Luna Universal One-Step Reaction Mix, 0.4 μL of 10 μM primers, 0.2 μL of 10 μM probe, and 1 μL of 20X Luna WarmStart® RT Enzyme Mix. These components were adjusted to a total reaction volume of 20 μL with RNase-free water. Amplification was conducted using the optimal thermocycling condition outlined in the manufacturer′s protocol for 40 cycles. The following primer-probe sets were used, targeting nsp14[18]: forward primer 5′-

TGG GGY TTT ACR GGT AAC CT-3′, reverse primer 5′- AAC RCG CTT AAC AAA GCA CTC-3′, probe 5′-56-FAM- FAM-TAGTTGTGA/ZEN/TGCWATCATGACTAG-3IABkFQ-3′. The standard curve was generated using qRT-PCR on serially diluted viral stock. The Ct values were then converted into viral titer (pfu/mL).

9. Statistical analysis

The results of multiple experiments are presented as the mean ± standard error of the mean (SEM). The statistical analysis was performed using a one-way analysis of variance followed by Tukey′s multiple comparison test as appropriate. This was conducted using GraphPad Prism 8 (GraphPad Software, Inc., La Jolla, CA, USA). $p < 0.05$ was considered statistically significant.

III. RESULTS

1. Activation of ARF1 is a crucial step for UPS of CFTR

UPS of CFTR occurs when ER stress exists in cells.[3] Therefore, to induce UPS of CFTR in controlled conditions, our methods included blocking of conventional trafficking[3] or treatment with the activator of IRE1α to induce ER stress in cells.[5] Overexpression of dominant-negative mutants of ARF1 (ARF1-Q71L, ARF1-T31N) can block conventional trafficking (Figure 1C and 1D), which can then induce protein accumulation in ER. However, as shown in Figure 1A and 1B, only ARF1-GTP restricted mutant (ARF1-Q71L) can significantly induce protein secretion of ΔF508-CFTR, and only a relatively small amount of CFTR was rescued to the plasma membrane when the ARF1-GDP restricted mutant (ARF1-T31N) was overexpressed. These results suggest that ARF1-GTP mediates unconventional trafficking of CFTR.

We investigated whether ARF1 is a crucial factor for UPS of CFTR using various methods to induce ER stress. First, SAR1-T39N and STX5 were used to block ER-to-Golgi trafficking,[19,20] (E)-2-(2-chlorostyryl)-3,5,6-trimethyl-pyrazine (CSTMP) was used as an IRE1α activator which is a sensor for ER stress and UPS of CFTR.[5] With ARF1 silencing, all of these methods resulted in decreased protein secretion of ΔF508-CFTR, demonstrating the importance of ARF1 in the process (Figure 2A-F). Then, to examine the occurrence of ARF1 activation under various ER stress-inducing conditions, an ARF1 activation assay was performed for those methods. GGA3, an adaptin that only interacts with ARF1-GTP forms, was utilized as bait for pull-down assays.[21] Activation of ARF1 was observed in all cells where UPS was induced (Figure 2G).

The most prominent role of ARF1 is to recruit coat protein complexes[22]. To investigate whether the activation of ARF1 is related to this process, we co-transfected cells with plasmids and siRNA targeting coat proteins known to be collected by ARF1. The giant proteins among each component of the complexes were selected as siRNA target molecules, and the efficacy of siRNA was measured using RT-qPCR (Figure 3C). The

results showed that none of these coat proteins are involved in the UPS of CFTR (Figure 3A and 3B).

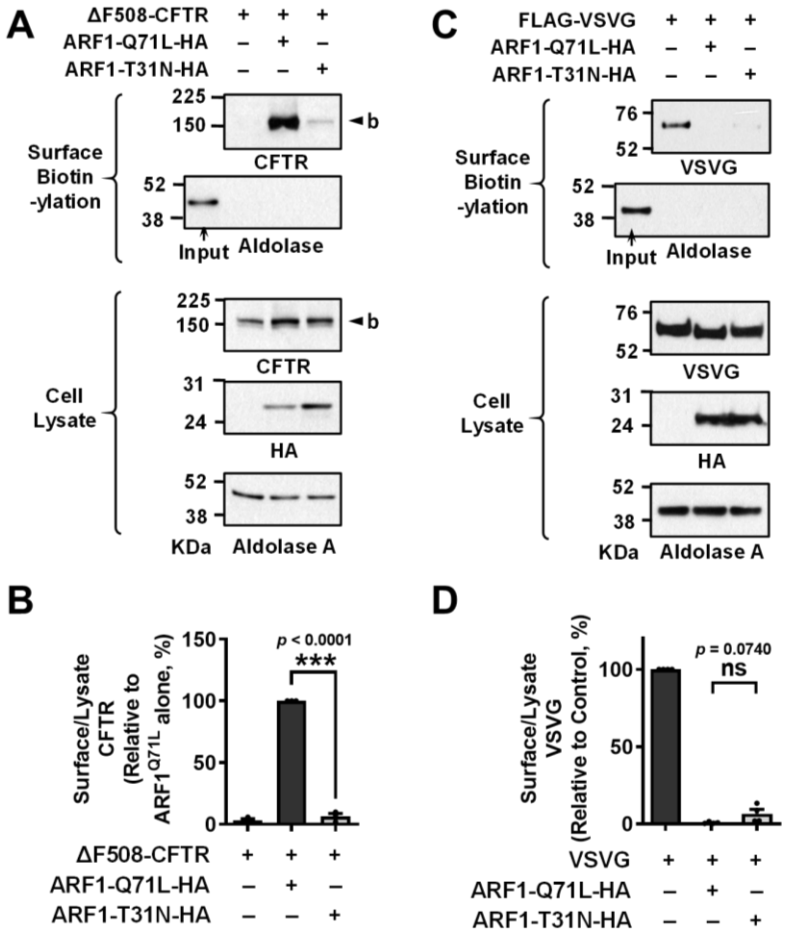

Figure 1. ARF1-GTP strongly induces UPS of CFTR, but ARF1-GDP does not. (A-B) UPS of ΔF508-CFTR induced by ARF1-Q71L is greater than that induced by ARF1-T31N. The cell surface biotinylation assay was performed in HEK293 cells transfected with ΔF508-CFTR, ARF1-Q71L, and ARF1-T31N. Cell surface proteins labeled with biotin and whole-cell lysates were immuno-blotted with the appropriate antibodies. Representative immunoblot images are shown in A, and quantifications of multiple experiments are summarized in B (n=3). (C-D) Both dominant-negative mutants block conventional trafficking. VSVG, ARF1-Q71L, and ARF1-T31N expressing plasmids were transfected in HEK293 cells. A surface biotinylation assay was conducted to analyze the surface

amount of VSVG, which is used as control cargo of conventional trafficking. Biotinylated surface proteins and whole cell lysates were blotted with the proper antibodies. Representative immuno-blot images are shown in C and quantitative results for immunoblots are summarized in D (n=4). Bar graph data are shown as mean ± SEM. *p < 0.05, **p < 0.01, ***p < 0.001, ns = not significant. Data were analyzed using one-way analysis of variance, followed by Tukey's multiple comparison test.

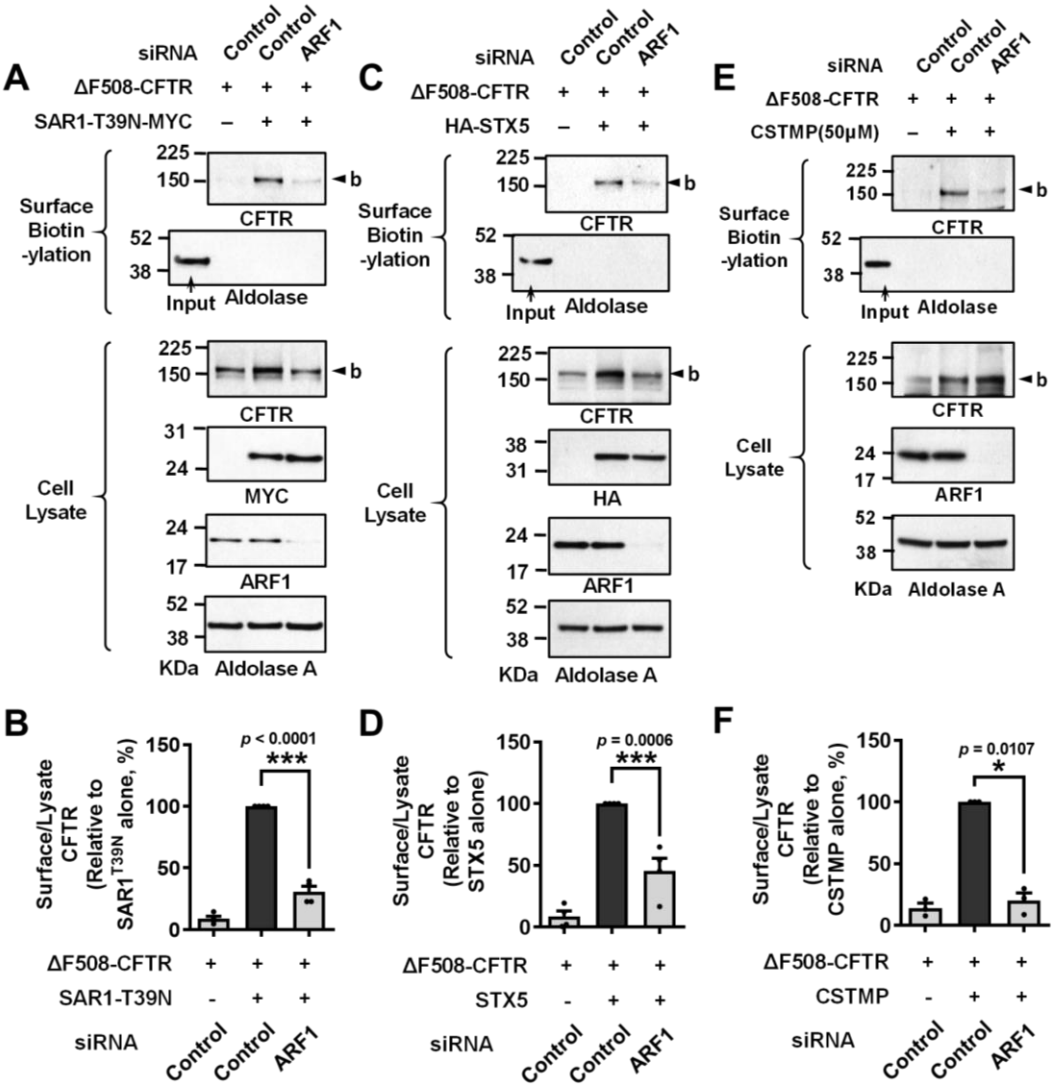

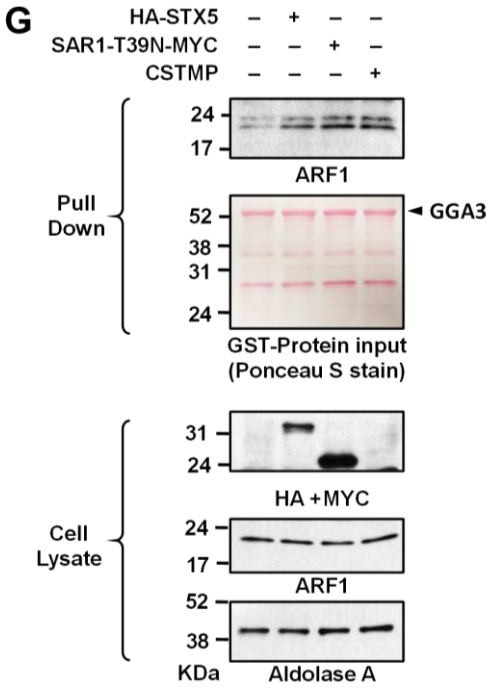

Figure 2. Activation of ARF1 is an essential step for UPS of CFTR. (A-F) UPS of ΔF508-CFTR was reduced when the ARF1 gene was silenced. A surface biotinylation assay was conducted with the ARF1 gene silenced. HEK293 cells were transfected with siRNA targeting ARF1 gene and scrambled siRNA as a control (50 nM, 48 hr). All cells were co-transfected with indicated plasmids or treated with CSTMP (50 μM, 12 hr). Immuno-blotting was performed with indicated antibodies. Representative immunoblots are shown in A, C, and E, and quantitative results are summarized in B, D, and F (n=3-4). (G) Activation of ARF1 is observed in various UPS induction methods. An ARF1 activation assay was conducted to analyze the activation level of ARF1. HEK293 cells were transfected with STX5, SAR1-T39N expressing plasmids or treated with CSTMP (50 μM, 12 hr). After 48 hours, cells were lysed and semi-pull-down assay was conducted with purified GGA3 protein tagged with GST. Representative results are shown in G. Bar graph data are shown as mean ± SEM. $*p < 0.05$, $**p < 0.01$, $***p < 0.001$. Data were analyzed using one-way analysis of variance, followed by Tukey's multiple comparison test.

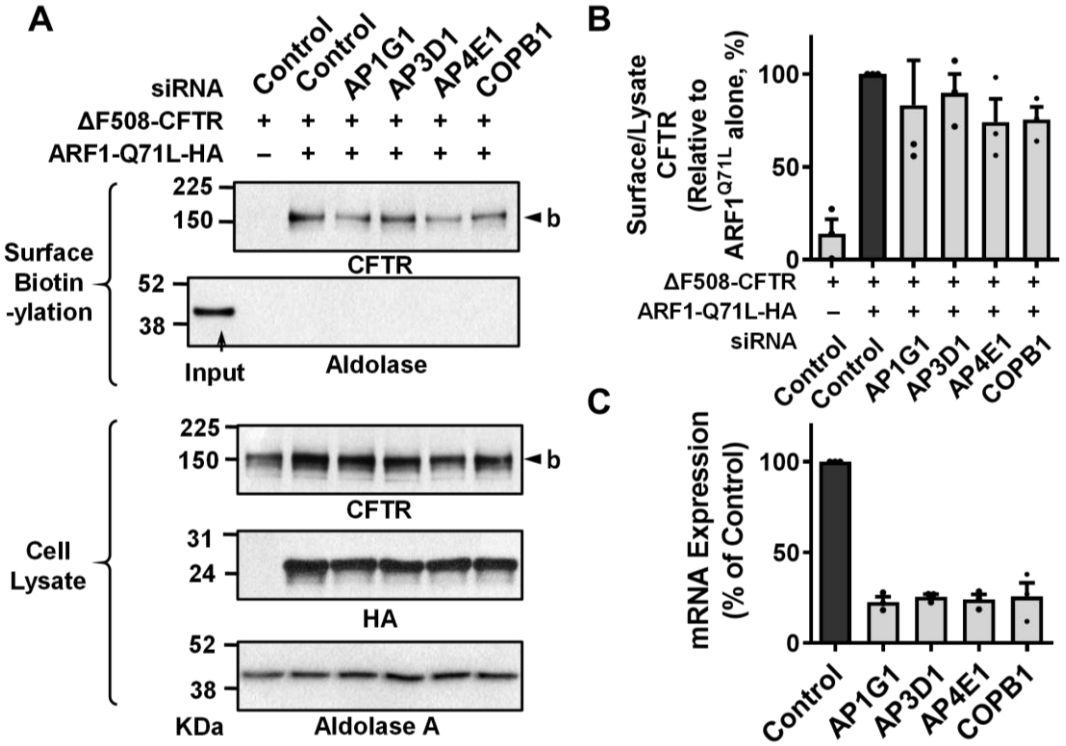

Figure 3. Activation of ARF1 is not for recruiting coat proteins in UPS of CFTR. (A-C) Gene silencing of coat proteins recruited by ARF1 did not affect the rescue of CFTR. Surface biotinylation assays were conducted with the gene silencing method (100 nM, 48 hr). SiRNA for target genes and control siRNA were transfected to HEK293 cells with ΔF508-CFTR and ARF1-Q71L expressing plasmids. The efficacy of siRNAs was confirmed with RT-qPCR. Representative blots are shown in A. Quantitative results were summarized in B-C (n=3). Bar graph data are shown as mean ± SEM.

2. Autophagy induced by ARF1-OSBPL1-VAPA complex mediates UPS of CFTR.

Since our results showed that the retained ΔF508-CFTR starts traveling from the ER,[23] we aimed to identify the ER-located molecules that interact with ARF1-GTP. One of the molecules is the vamp-associated protein (VAP), which is also known to contribute to autophagosome formation. Autophagosome formation is associated with UPS.[24] To investigate whether these genes are involved in the mechanism, cell surface biotinylation assays were performed with gene silencing of VAP. As shown in Figure 4A and 4B, when the VAPA gene was silenced, the rescue of ΔF508-CFTR was suppressed. In contrast, with the knockdown of VAPB, UPS of ΔF508-CFTR was greater than in the control group. In addition, overexpression of VAPA synergistically rescued CFTR to the plasma membrane with ARF1-Q71L (Figure 4C and 4D). Immunoprecipitation was performed to examine the protein-protein interaction between ARF1 and VAPA. Only the ARF1-GTP mutant interacted with VAPA, which explains how activated ARF1 plays a role in UPS (Figure 5A and 5B).

In general, ARF1 and VAPA interact by forming a complex with an oxysterol-binding protein (OSBP) which has both an ARF1-binding PH domain and a VAP-binding FFAT domain.[14] Target genes were selected for the assay among the OSBP gene family with both PH and FFAT domains (Figure 6). The surface biotinylation assay with silencing of OSBP family genes revealed that OSBPL1 mediates UPS of ΔF508-CFTR (Figure 7A-B). The efficiency of siRNA in each target molecule was evaluated using RT-qPCR (Figure 7C). Because ARF1-OSBPL1-VAPA complex formation is more likely without OSBP, ΔF508-CFTR was more effectively rescued as a result of OSBP gene silencing.

VAPA interacts directly with multiple autophagy-related genes and contributes to the autophagosome formation.[24] Therefore, we examined whether the complex formed by ARF1 activation is related to autophagosome formation. The LC3 lipidation level, an indicator of autophagosome formation,[25] was observed in cells expressing ARF1 mutations. Lipidation of LC3 significantly increased with ARF1-Q71L overexpression (Figure 8A and 8B, second lane). With ARF1-T31N overexpression, only a small amount

of LC3 lipidation was observed compared to ARF1-Q71L (Figure 8A and 8B, third lane). A similar phenomenon was observed in immunofluorescence. LC3 puncta, a marker for autophagosome in immunofluorescence, was observed when ARF1-Q71L was overexpressed in cells. CFTR colocalized with the LC3 puncta (Figure 8C).

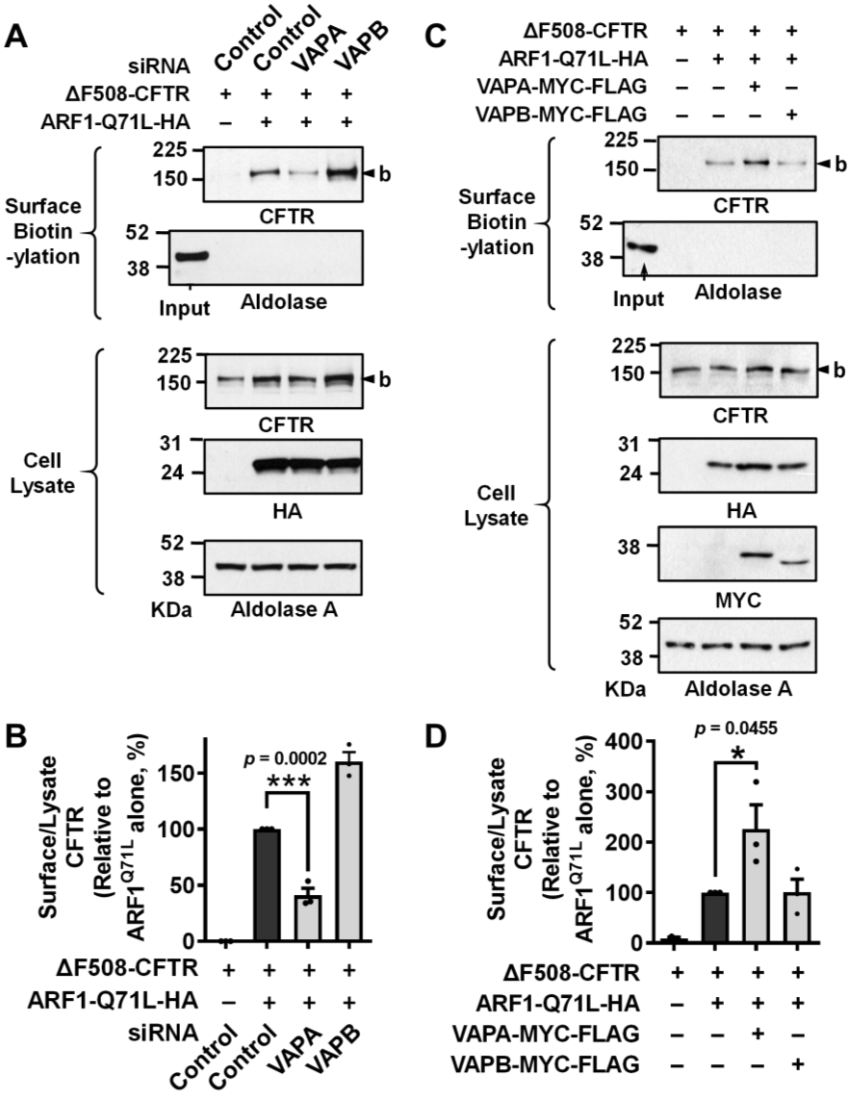

Figure 4. VAPA is involved in the UPS of CFTR. (A-B) Knockdown of VAPA gene partially reduced UPS of ΔF508-CFTR. Surface biotinylation analysis was conducted to observe changes in surface expression of ΔF508-CFTR with HEK293 cells transfected with siRNAs or annotated plasmids. Representative blots are shown in A, and Quantifications of multiple experiments were summarized in B (n=3). (C-D) Overexpression of VAPA

synergically induced rescue of CFTR to the plasma membrane with ARF1-Q71L. Surface biotinylation analysis was conducted to observe changes in CFTR surface expression with HEK293 cells transfected with annotated plasmids. Representative blots are shown in C, and Quantifications of multiple experiments were summarized in D (n=3). Bar graph data are shown as mean ± SEM. *$p < 0.05$, **$p < 0.01$, ***$p < 0.001$. Data were analyzed using one-way analysis of variance, followed by Tukey's multiple comparison test.

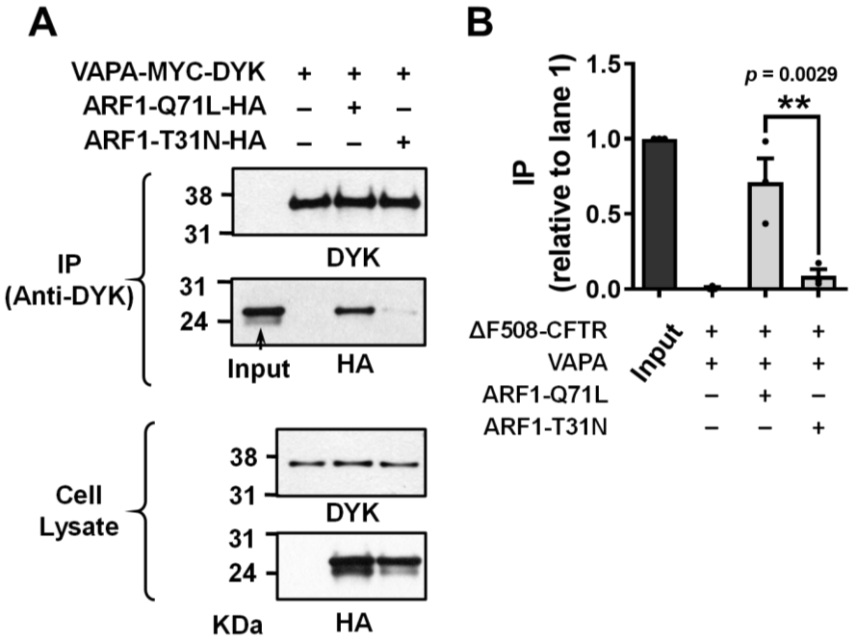

Figure 5. Interaction between ARF1 and VAPA Activated ARF1 interacts with VAPA. Immunoprecipitation was performed to analyze the interaction between ARF1 and VAPA in HEK293 cells. Cell lysates were precipitated with anti-DYK and blotted with HA antibodies. Representative blots are shown in A. Quantifications of multiple experiments were summarized in B (n=3). Data are shown as mean ± SEM. *$p < 0.05$, **$p < 0.01$, ***$p < 0.001$. Data were analyzed using one-way analysis of variance, followed by Tukey's multiple comparison test.

Figure 6. Structural organization of OSBP family based on the domains. OSBPL2, OSBPL10, and OSBPL11 cannot act as a bridge between ARF1 and VAPA because they do not have either a PH domain (ARF1 interacting region) or an FFAT domain (VAPA interacting region).

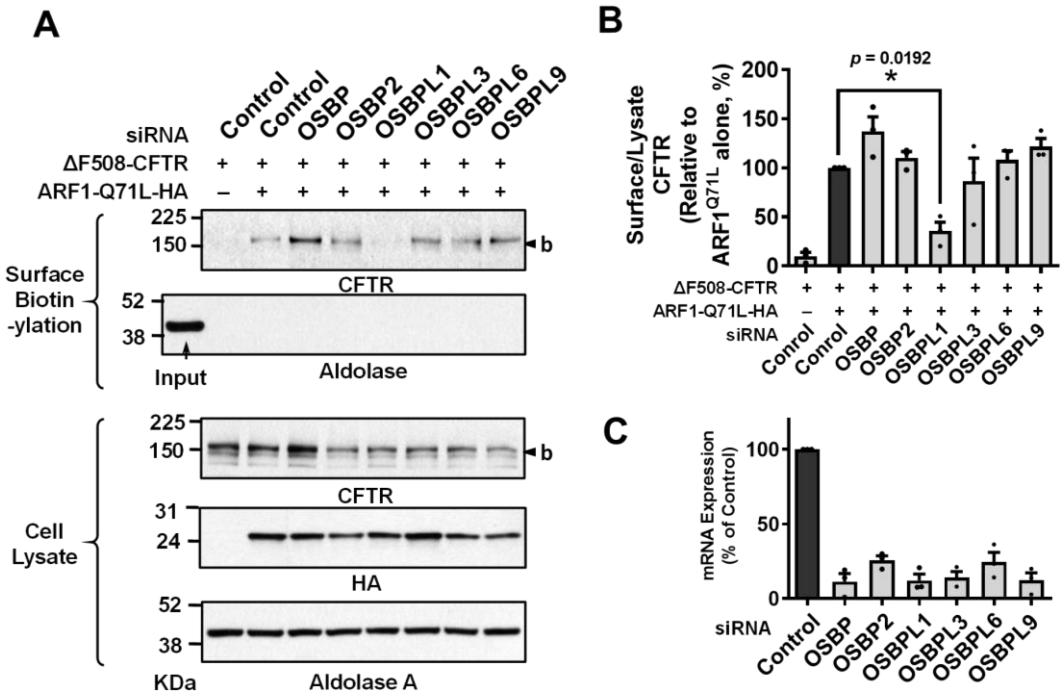

Figure 7. Knockdown of OSBPL1 gene reduced surface expression of ΔF508-CFTR. (A-B) HEK293 cells co-transfected with siRNAs, ΔF508-CFTR, and ARF1-Q71L were surface biotinylated and analyzed via immunoblotting (C) RT-qPCR was used to measure the efficacy of each siRNA. Representative blots are shown in A, and Quantifications of multiple experiments were summarized in B and C (n=3). Bar graph data are shown as mean ± SEM. *$p < 0.05$, **$p < 0.01$, ***$p < 0.001$. Data were analyzed using one-way analysis of variance, followed by Tukey's multiple comparison test.

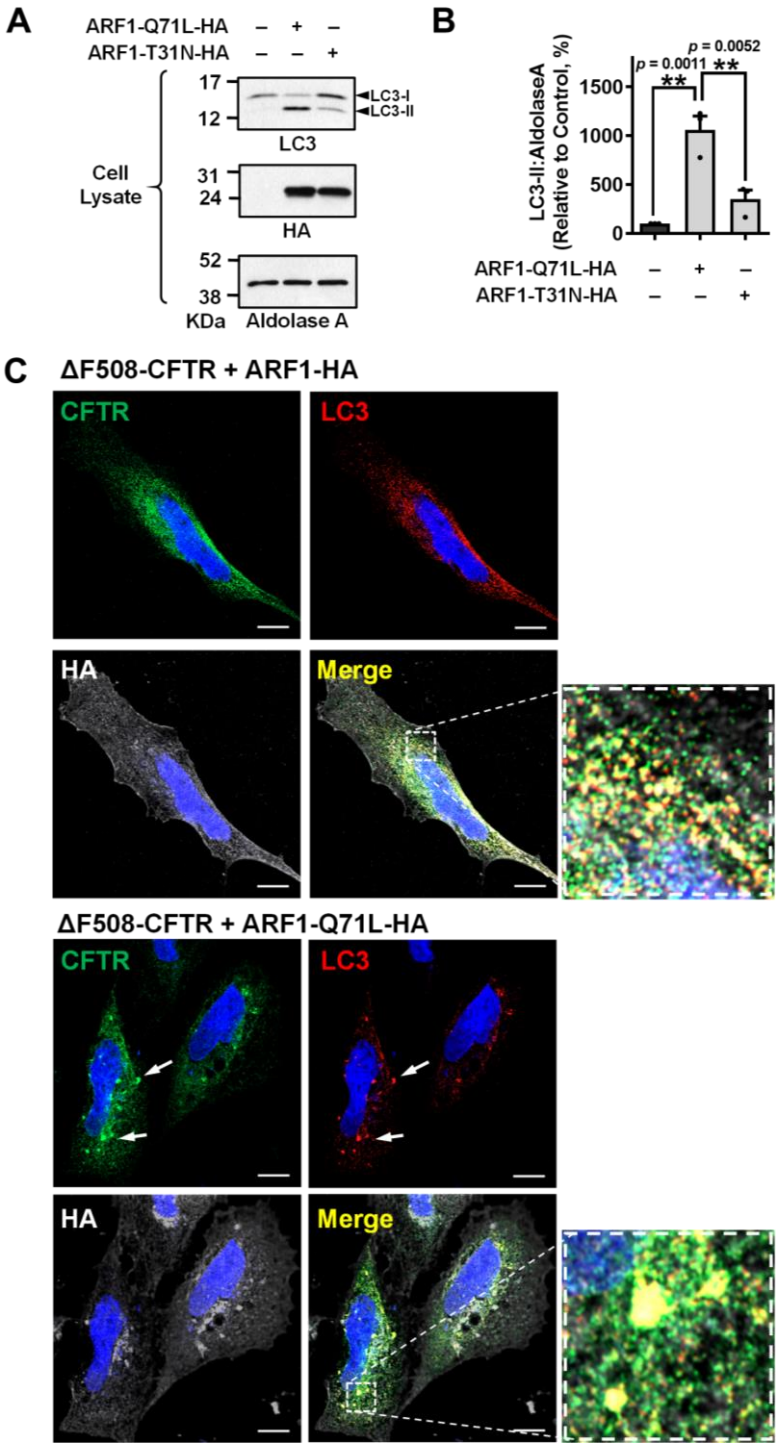

Figure 8. ARF1-Q71L induces autophagosome formation. (A-B) Overexpression of ARF1-Q71L induces lipidation of LC3, an autophagosome marker. Lipidation of LC3 was analyzed in HEK293 cells transfected with ARF1-Q71L and ARF1-T31N. Representative immunoblots detected with LC3 are shown in A, and the results of multiple experiments are summarized in B (n =3). (C) Overexpression of ARF1-GTP restricted mutant induces formation of LC3 puncta which is marker for autophagosome. HeLa cells transfected with ΔF508-CFTR, ARF1-HA, or ARF1-Q71L-HA were used. ΔF508-CFTR was stained with anti-CFTR antibodies with green fluorophore-tagged secondary antibodies. ARF1-HA and ARF1-Q71L-HA were stained with anti-HA antibodies with red fluorophore-tagged secondary antibodies. LC3 was stained with anti-LC3 antibodies with far-red fluorophore-tagged secondary antibodies. Bar graph data are shown as mean ± SEM. *$p < 0.05$, **$p < 0.01$, ***$p < 0.001$. Data were analyzed using one-way analysis of variance, followed by Tukey's multiple comparison test.

3. Activation of ARF1 Mediates UPS of SAS-CoV-2 Spike

In light of the COVID-19 pandemic, understanding its mechanism of viral replication and assembly in host cells is of paramount importance. This study tested the hypothesis that SARS-CoV-2 S protein travels through UPS, bypassing the Golgi apparatus.[26] Since S protein has a furin cleavage-site present at the S1/S2 junction, it can be cut by furin enriched in the Golgi apparatus. Thus the full-length and the cleaved S protein are both observed in cell lysates.[10] In control experiments, the localization of furin was not changed by SARS-CoV-2 infection (Figure 9).

When overexpressing codon-optimized S protein in HEK293 cells, most of the S proteins on the surface had been cleaved because they were traveling through conventional protein secretion via the Golgi apparatus (Figure 10A and 10B, first lane). The full-length form of S protein was observed on the surface when ER-to-Golgi blockade by ARF1-Q71L occurred. This indicates that S protein had traveled via UPS and bypassed the Golgi apparatus (Figure 10A and 10B, second lane). By contrast, when ARF1-T31N induced ER-to-Golgi blockade, full-length S protein was not observed on the cell surface, showing that unconventional trafficking of S protein is also associated with activated ARF1 (Figure 10A and 10B, third lane).

Among the SARS-CoV-2 virus genes, ORF3a can evoke ER stress in host cells.[27] ORF3a is a viroporin that interferes with ion channel activities in host plasma and endomembranes.[28] As shown in Figure 10C-F, phosphorylation of IRE1α and UPS of S protein were induced in response to ORF3a expression, allowing full-length S protein to be observed on the surface. However, with ARF1 gene silencing, ORF3a-induced UPS of S protein was reduced, indicating that ARF1 is also involved in the trafficking of S protein.

Then, the trafficking of S protein was investigated in authentic SARS-CoV-2 virus. HEK293T cells were used for transfection of exogenous plasmids, and HEK293T cells expressing ACE2 and TMPRSS2 were used to infect the virus. ACE2 and TMPRSS2 are required as S protein receptors and S protein-activating enzymes, respectively, for SARS-

CoV-2 viral infection in the host cell.[9] Cells infected with authentic SARS-CoV-2 virus expressed ORF3a at a level 3.2 times higher than that of exogenous ORF3a-expressing plasmids, which led to much stronger phosphorylation of IRE1α (Figure 11). This robust ER stress activation was associated with higher levels of uncleaved S protein in the SARS-CoV-2 viruses collected from supernatants of infected cells (Figure 11C and 11D).

To identify the molecular mechanism of protein trafficking of SARS-CoV-2, we observed protein secretion of S proteins and viral replication of SARS-CoV-2 in the absence of several genes that have been reported as UPS-related genes. GRASP55 and Transmembrane P24 Trafficking Protein (TMED) interact directly with UPS cargo and support protein secretion under ER stress conditions.[3,15] HEK293 cells were used to transfect plasmids, and Vero cells endogenously expressing ACE2 were used to investigate the replication of the authentic virus. Silencing these genes hinders ORF3a-induced UPS of S protein and SARS-CoV-2 replication, demonstrating that trafficking of SARS-CoV-2 S is linked to UPS (Figure 12).

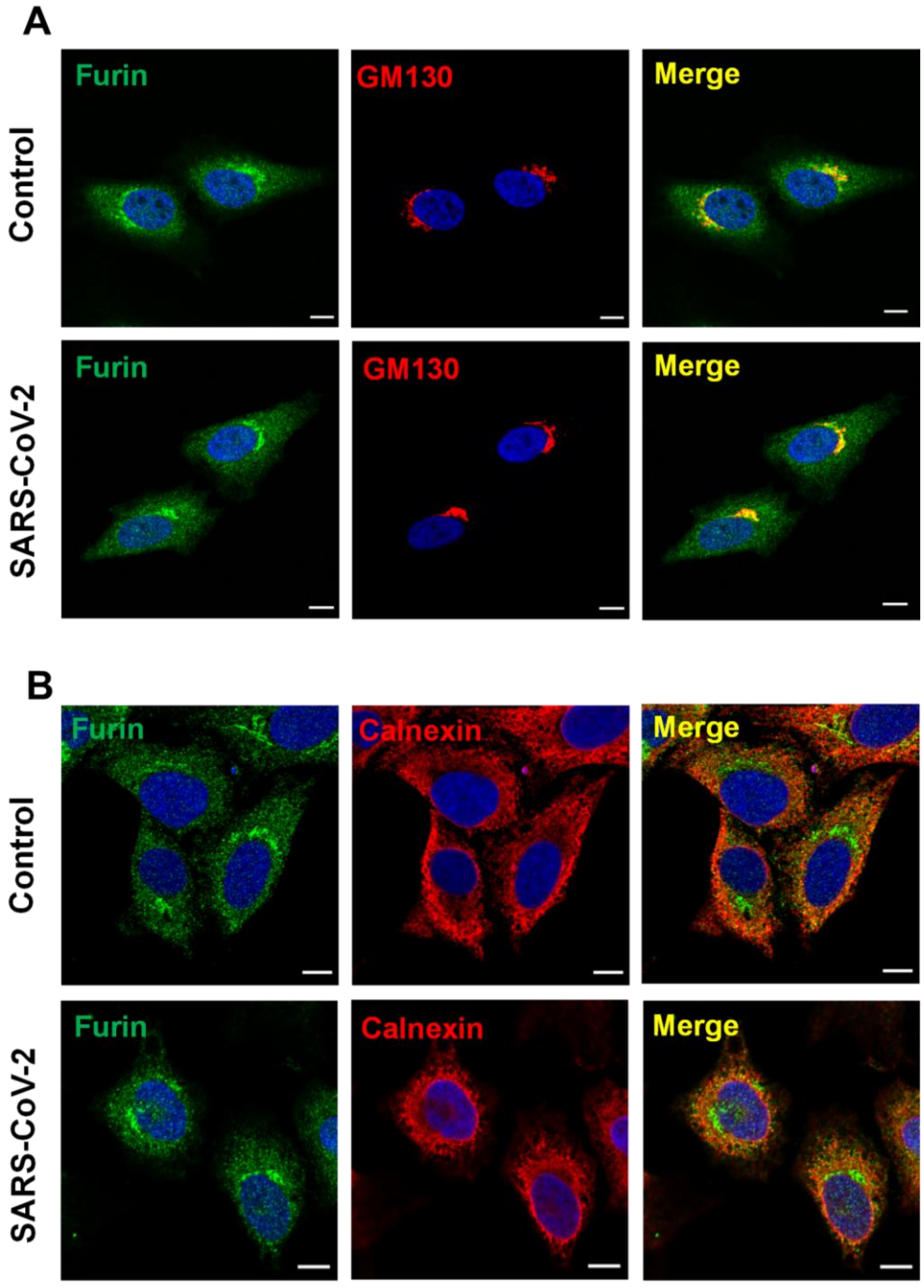

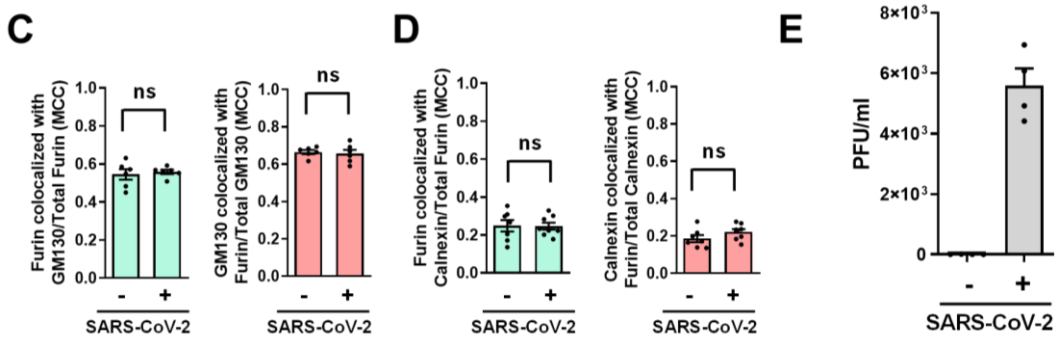

Figure 9. SARS-CoV-2 infections do not affect the cellular localization of furin. The cellular localization of furin was analyzed using immunofluorescence in HeLa cells stably expressing ACE2 (HeLa-ACE2) with or without SARS-CoV-2 infection. Furin was labeled with anti-Furin antibodies with green fluorophore-tagged secondary antibodies. (A-B) Immunofluorescence images of the Golgi complex was labeled with anti-GM130 antibodies with red fluorophore-tagged secondary antibodies after permeabilization. Quantification of colocalization between furin and GM130 using the Manders′ colocalization coefficient (MCC) is summarized in B (n=6). (C-D) Immunofluorescence images of the ER was labeled with anti-calnexin antibodies with red fluorophore-tagged secondary antibodies after permeabilization. Representative immunofluorescence images are shown in C. Quantification of colocalization between furin and calnexin using MCC is summarized in D (n=7-8). The Golgi localization of furin is not significantly altered during SARS-CoV-2 infections. (E) The SARS-CoV-2 infections in HeLa-ACE2 cells were confirmed by quantifying viral RNA in the cell culture supernatant. Cells were infected with 0.01 MOI SARS-CoV-2, and the culture supernatant was harvested at 24 hr post-infection. The Ct values of quantitative PCR were converted into viral titer (pfu/mL). Bar graph data are shown as mean ± SEM. ns = not significant. Data were analyzed using a two-tailed Student′s t-test.

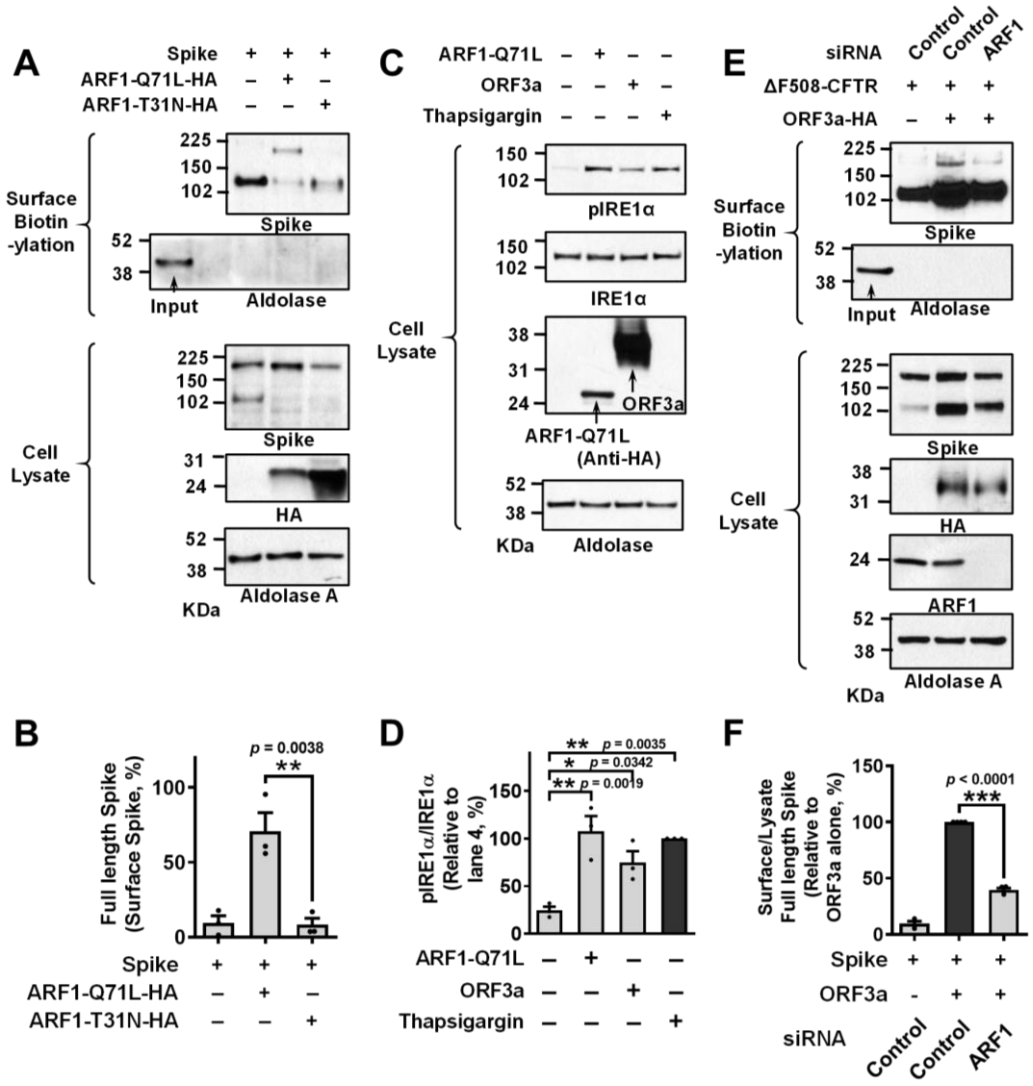

Figure 10. ARF1 mediates UPS of SARS-CoV-2 S protein. (A-B) The ARF1-Q71L induces UPS of SARS-CoV-2 S protein, but ARF1-T31N does not. The cell surface expression of uncleaved and cleaved S proteins was analyzed using surface biotinylation assays in HEK293 cells. Representative surface biotinylation assays are shown in A, and the results of multiple experiments are summarized in B (n=3). (C-D) The SARS-CoV-2 ORF3a induces ER stress. Phosphorylation of IRE1α, a marker of ER stress, was analyzed

in HEK293 cells transfected with ARF1-Q71L and ORF3a (24 hr). Thapsigargin (2 μM, 6 hr) was used as a positive control to induce ER stress. Representative immunoblots are shown in E and the results of multiple experiments are summarized in F (n=3). (E-F) Uncleaved S proteins were shown on the cell surface by ORF3a-induced ER stress but decreased when ARF1 gene was silenced (n=3). Bar graph data are shown as mean ± SEM. $*p < 0.05$, $**p < 0.01$, $***p < 0.001$. Data were analyzed using one-way analysis of variance, followed by Tukey's multiple comparison test.

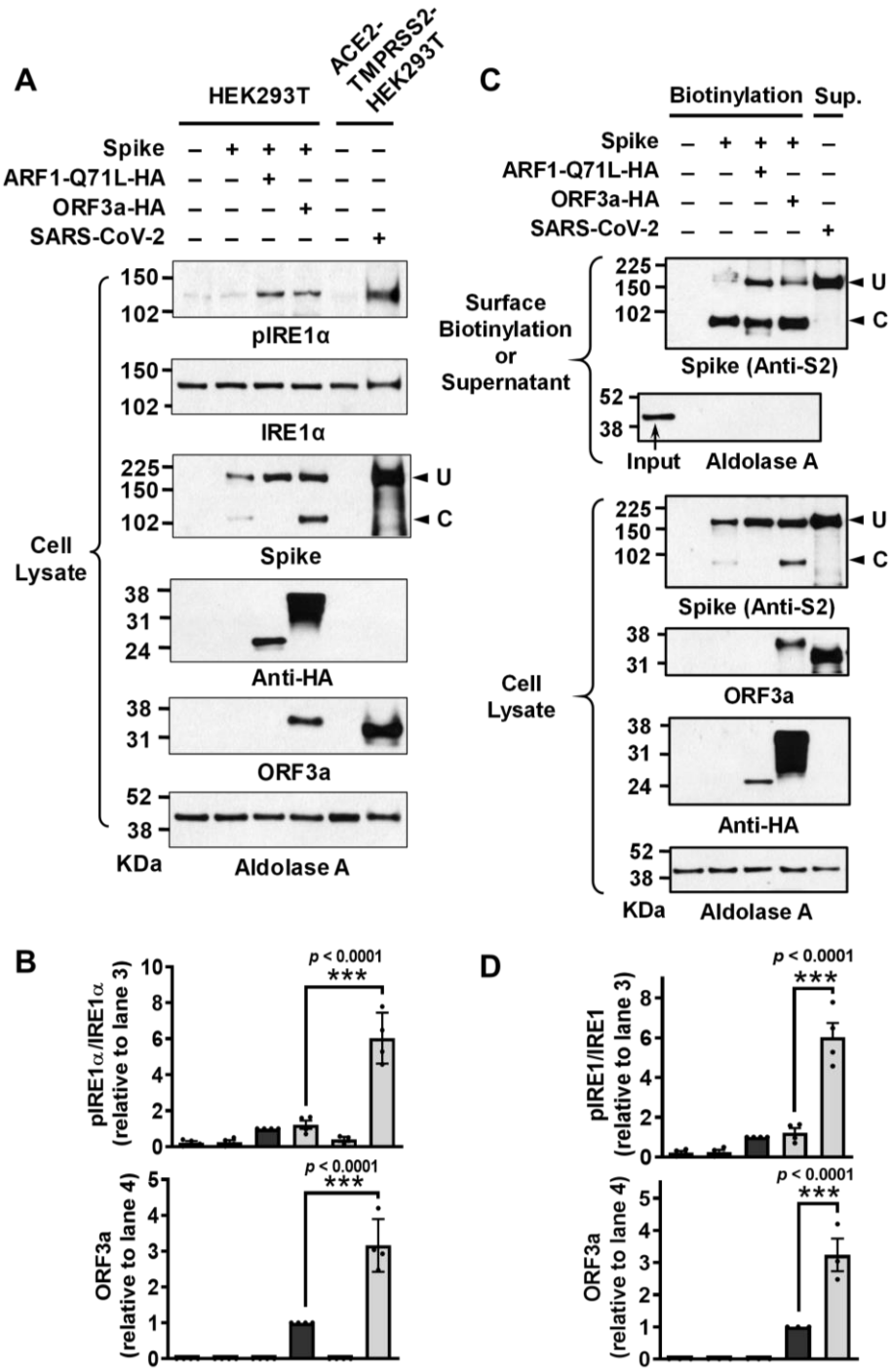

Figure 11. Trafficking of S protein in the authentic SARS-CoV-2 viruses. (A-B) The authentic SARS-CoV-2 virus infection evoked higher levels of ORF3a expression and IRE1α phosphorylation than the ORF3a plasmid transfection. IRE1α phosphorylation and ORF3a expression were analyzed in HEK293T cells transfected with the indicated plasmids (lanes 1–4) or those with authentic SARS-CoV-2 infection (lane 6). HEK293T cells stably expressing ACE2 and TMPRSS2 (ACE2-TMPRSS2-HEK293T) were used for the SARS-CoV-2 infection. Representative immunoblots detected with anti-phospho IRE1α or anti-ORF3a are shown in A, and the results of multiple experiments are summarized in B (n=3–4). (C-D) The SARS-CoV-2 virions contain a higher level of uncleaved S. The expression of S protein on the cell surface or viral particle was analyzed. Cell surface biotinylation immunoblots performed on HEK293T cells transfected with the indicated plasmids (Biotinylation). The SARS-CoV-2 virions were harvested from the supernatant of infected ACE2-TMPRSS2-HEK293T cells (Sup). Representative immunoblots are shown in C, and the results of multiple experiments are summarized in D (n=4). Bar graph data are shown as mean ± SEM. $*p < 0.05$, $**p < 0.01$, $***p < 0.001$. Data were analyzed using one-way analysis of variance, followed by Tukey's multiple comparison test.

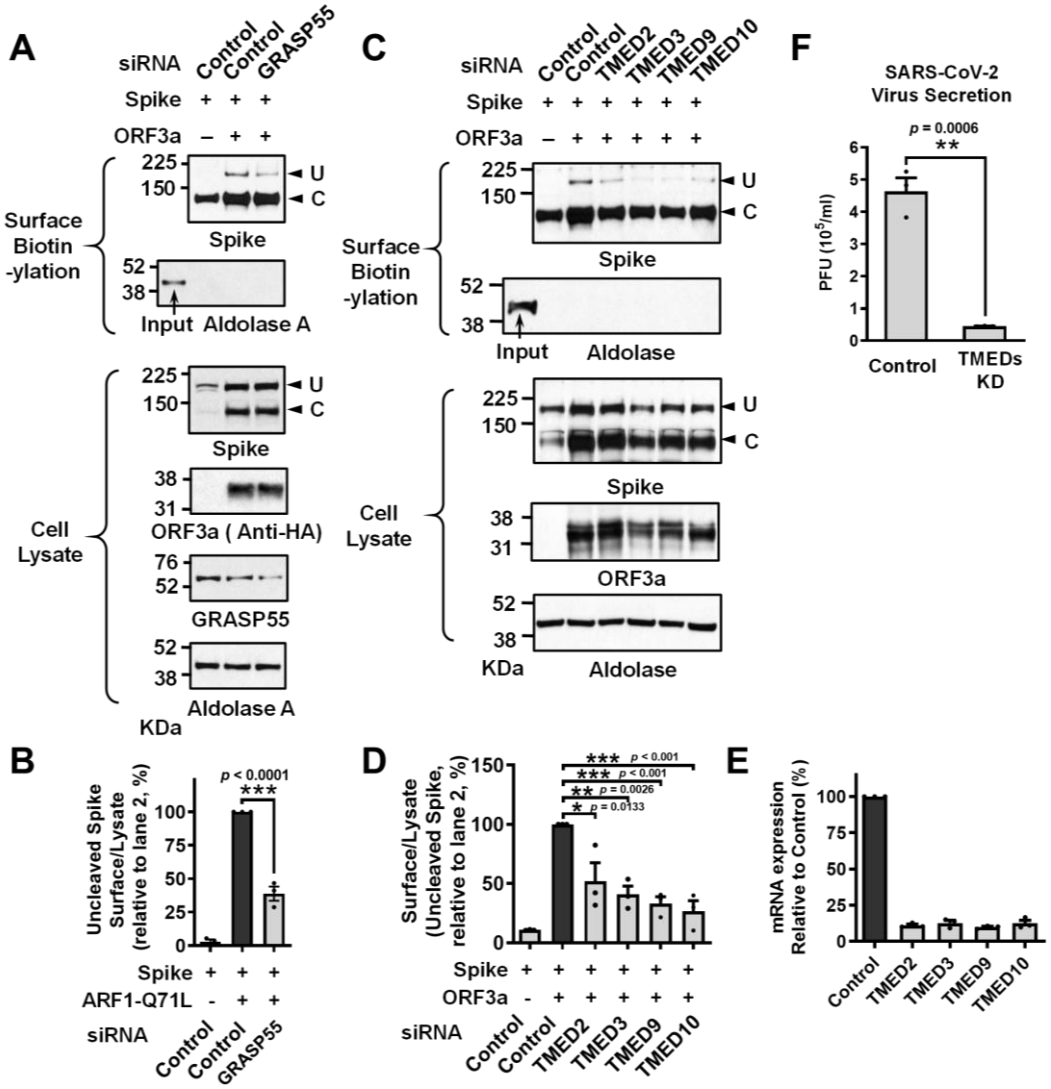

Figure 12. Silencing UPS-related genes inhibits UPS of S protein. (A-B) Silencing of GRASP55 partially inhibits ORF3a-induced UPS of S protein. The effects of GRASP55 gene silencing (100 nM, 48 hr) on the cell surface expression of S protein were analyzed with co-expression of SARS-CoV-2 ORF3a. Representative blots of surface biotinylation assays are shown in A, and the results of multiple experiments are summarized in B (n=3).

(C-D) Effects of individual TMED (TMED2, 3, 9, and 10) gene silencing (100 nM each, 48 hr) on the ORF3a-induced UPS of SARS-CoV-2 S were analyzed. The cell surface expression of uncleaved (U) and cleaved (C) S protein was analyzed using surface biotinylation assays in HEK293 cells. Representative blots of surface biotinylation assays are shown in C, and the results of multiple experiments are summarized in D (n=3). (E) Viral RNA in the cell culture supernatant was analyzed using quantitative PCR. Vero cells were infected with 0.01 MOI SARS-CoV-2, and the culture supernatant was harvested at 24 hour post-infection. Bar graph data are shown as mean ± SEM. *$p < 0.05$, **$p < 0.01$, ***$p < 0.001$. Data were analyzed using a two-tailed Student's t-test or one-way analysis of variance, followed by Tukey's multiple comparison test.

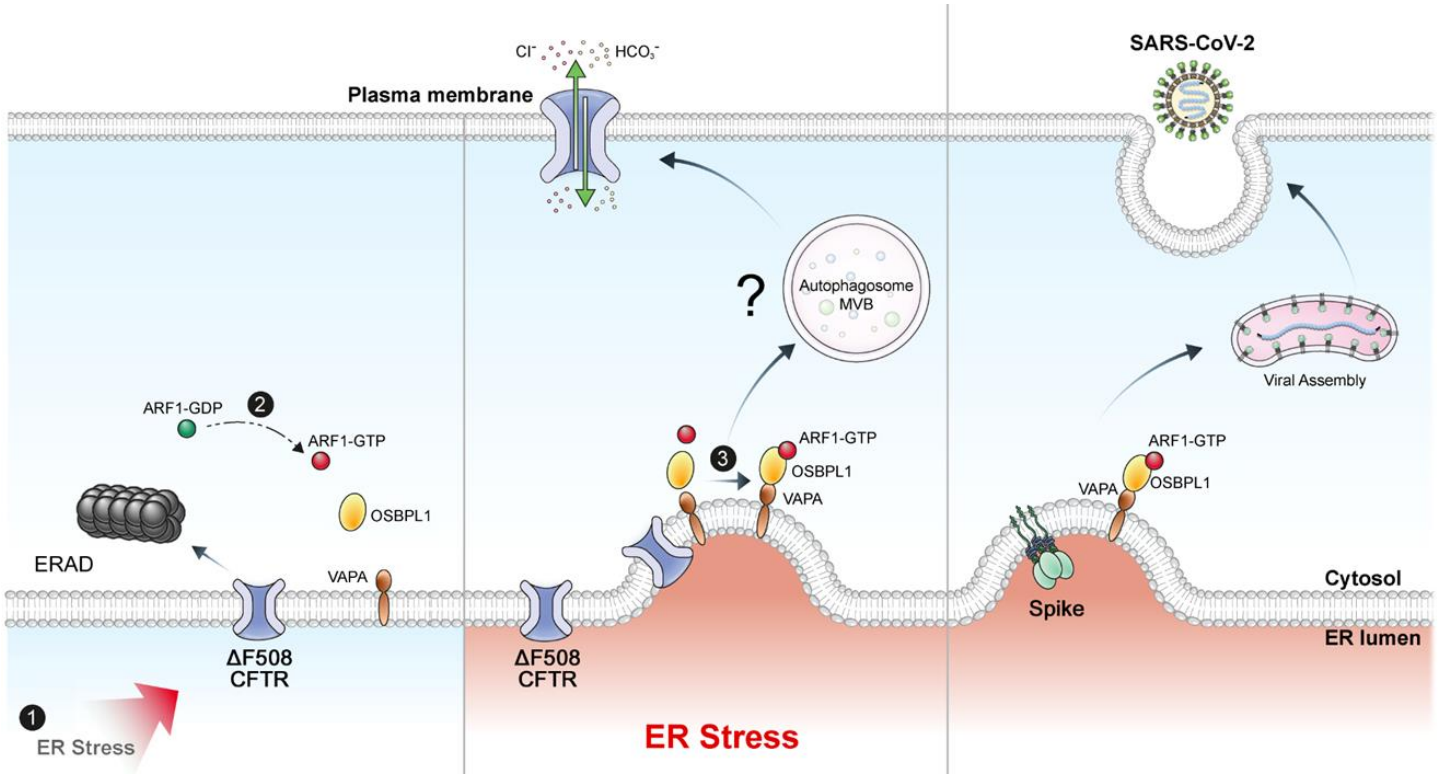

Figure 13. Graphic depiction of ARF1-mediated UPS of ΔF508-CFTR and SARS-CoV-2 S protein. Activated ARF1 forms a complex with OSBPL1 and VAPA and triggers UPS by inducing autophagosome formation. This process confirms the vital role of ARF1 in the UPS of clinically important transmembrane proteins

IV. DISCUSSION

UPS has been the subject of intense research recently. Several cargoes have been found to move via this pathway, and many factors involved in this mechanism have been identified.[2] Moreover, It was discovered that multiple viruses replicate along this pathway.[26] However, the underlying mechanism has not yet been elucidated. This study revealed the role of ARF1 in UPS of CFTR and SARS-CoV-2 S protein. The results showed that activation of ARF1 is a necessary step for UPS (Figure 2), and ARF1-OSBPL1-VAPA complex promotes UPS by evoking autophagosome formation (Figure 8). Moreover, S proteins in authentic virus traveled through the Golgi-bypassing route evoked by ORF3a-induced ER stress (Figure 8 and 9). A graphical summary of this mechanism is illustrated in Figure 13. This study shows the specific mechanism of UPS of CFTR and S protein related to ARF1, however, whether there is a direct interaction between ARF1, OSBPL1, and VAPA is should be verified with a pull-down assay in the following study.

Autophagy, which once held the view of a degradative system,[29,30] was found to serve as a secretory pathway as well as degradation.[31] Several studies have shown that secretory autophagy facilitate UPS of leaderless cytosolic proteins.[32] In our previous work, specific autophagy components participate in UPS of CFTR.[4] Moreover, overexpression of ARF1-Q71L causes autophagosome accumulation, which is related to secretory pathway, not for degradation.[4] The autophagosome accumulation was significantly increased with ARF1-Q71L overexpression, and only a small amount was observed when ARF1-T31N was overexpressed (Figure 8). This study demonstrates that activation of ARF1 evokes autophagosome formation contributing UPS of CFTR through interaction with VAPA.

ARF1-OSBPL1-VAPA complex leads to autophagosome formation in ER (Figure 8), but ARF1 mainly localizes to ERGIC and the Golgi apparatus. Some questions still remains about where ARF1 interacts with VAPA. There are two possibilities. First, a small amount of ARF1 in the ER induces UPS. Although the data is not shown here, localization of ARF1 appeared in ER in early stage (~6 hr). This result suggests that ARF1 plays a role in ER

and may form MCS between ER and autophagic vacuoles derived from the ER membrane.[33,34] The other possibility is that ARF1, located in ERGIC or Golgi apparatus, forms the ARF1-OSBPL1-VAPA complex in ER, creating a MCS between ER-ERGIC or ER-Golgi. The most prominent role of the ARF1-OSBP-VAP complex is membrane tethering between ER-Golgi to transport lipids between them.[14,35] Cholesterol, which causes membrane stiffness[36] and makes the membrane difficult to bend, transports from ER to Golgi using this complex. Moreover, PI4P, a signal related to the autophagosome biogenesis[37] and the fusion of autophagosomes and lysosomes,[38] transports from the Golgi apparatus to ER with ARF1-OSBPL1-VAPA complex.[14] Several viruses using UPS, such as enterovirus and hepatitis C virus, accumulate PI4P in virus assembly site in host cell.[39,40] This lipid movement may support the biogenesis of UPS vesicles in ER. Since there are many possible explanations, more research is needed to understand the exact mechanism.

Although previous studies have described the interaction between ARF1 and TMEDs,[41] this study did not observe interaction between ARF1 and TMEDs, the cargo receptors for CFTR and S protein in UPS.[15] The interaction between these two molecules was observed in the biogenesis of COPI vesicles.[41] However, in this study, activated-ARF1 did not play a role in recruiting coat proteins in UPS (Figure 3). It is difficult to confirm whether or not there is an interaction between ARF1 and TMEDs, since ARF1 does not directly generate vesicles as previously reported. Although the prominent role of TMEDs in UPS is the cargo receptor, TMED2 and TMED10 also play a role in assembling ARF1, OSBP, and VAPA complex.[42] The correlation between ARF1 and TMEDs should be further investigated in following studies.

The results of gene silencing showed that VAPB is not required for the secretion of ΔF508-CFTR, but VAPA is (Figure 4A and 4B). Moreover, only overexpression of VAPA synergistically rescues CFTR to the plasma membrane with ARF1-Q71L (Figure 4C and 4D). The difference between these two genes is of particular interest in understanding this mechanism. VAPs are ubiquitous proteins mainly localized in ER[43] and are involved in various cellular mechanisms such as membrane contact site,[44] vesicular trafficking,[45]

unfolded protein response,[46,47] and autophagosome formation.[24,48] VAPA and VAPB share 63% sequences,[49] both VAPs are involved in the autophagosome biogenesis in ER,[24] and both can organize the VAP-OSBP-ARF1 complex.[35] However, they have different expression levels in various tissues and distinct interactome in cells.[50] Functional variations between the genes were not verified until now, and further study should be conducted to investigate the functional differences between them.

Of the OSBP family, only OSBPL1 contributes to ΔF508-CFTR protein secretion. (Figure 7). Moreover, only OSBPL1 has an ankyrin domain (Figure 6). The ankyrin domain consists of ankyrin tandem repeats mediating protein-protein interaction.[51] The ankyrin in OSBPL1 interacts with Ras-related protein Rab-7 (RAB7) in the late endosome.[52] Interaction between OSBPL1 and RAB7 occurs in the middle of ER and late endosomes and forms a membrane contact site between them.[52] Recent studies have revealed that late endosomes, which RAB7 localizes, are related to the unconventional secretion of misfolded proteins.[53] This study demonstrates that OSBPL1 not only forms an ARF1-OSBPL1-VAPA complex but can also interact with RAB7 and help regulate late endosomes in UPS.

Analysis of the interactome of ARF1 and VAPA in the open source database (BioGRID) reveals that several SARS-CoV-2 viral proteins interact with both ARF1 and VAPA.[54] In addition to the ORF3a mentioned in the study, an envelope protein (E), membrane glycoprotein (M), ORF6, ORF7a, and ORF7b interact with both ARF1 and VAPA.[54] E and M are the structural protein of SARS-CoV-2,[55] which travel to the virus assembly site, the double-membrane vesicle (DMV).[56] ORF7a and ORF7b are also structural accessory proteins[56] that may be collected at the DMV. ORF6 primarily localizes in ER and autophagosome membranes,[57] which can help deliver viral structural proteins to DMVs. These findings demonstrate that ARF1 and VAPA are required for viral replication, and virus replication occurs through UPS.

Why SARS-CoV-2 uses UPS for replication remains elusive. Most groups that use these pathways are positive-stranded RNA viruses such as poliovirus, enterovirus and influenza A virus.[32] They probably create optimal conditions to replicate in the host cells, such as ER

reorganization,[58] using their fast protein expression. In addition, pre-cleavage of S1/S2 before egress may affect their infectivity due to loss of ACE2 receptor binding site. SARS-CoV-2 viruses seem to use various routes for their replication as well as Golgi-bypassing UPS pathway.[9,15,59] This is probably because SARS-CoV-2 diversifies the glycosylation pattern of the S protein for their immune evasion in host cell.[60]

In the present study, several methods were utilized to induce ARF1-activated UPS in cells (Figure 2G). In prior research, ER-to-Golgi blockade caused phosphorylation of IRE1α,[5] which affects the activation of ARF1 in cancer.[61] Phosphorylated IRE1α activates SRC tyrosine kinase, which activates Golgi-associated BFA-resistant Guanine Nucleotide Exchange Factor 1 (GBF1).[61] GBF1 is required for ARF1 activation.[62] Moreover, ER stress-induced re-localization of ER chaperones in the plasma membrane is a typical phenotype of tumor cells associated with regulating oncogenic signal pathway, immunity, and proliferation.[63,64] Some of these ER chaperones can be secreted through UPS.[65] Further research is needed to determine whether the re-localization of ER chaperones occurs through UPS. If so, this study may provide important information for the development of new therapeutic targets for cancer cells.

In conclusion, this study revealed that ARF1 plays a critical role in the UPS of CFTR and SARS-CoV-2. In addition, it provides evidence of its applicability to new therapeutic strategies for cystic fibrosis and COVID-19. Further research is needed to better understand how ER stress affects ARF1 activation, how autophagosome cargo travels to the plasma membrane, and whether the same mechanism applies to other secretory cargoes.

V. CONCLUSION

The underlying mechanism for UPS of transmembrane proteins and viral replication of SARS-CoV-2 has not yet been elucidated. This study provides novel insight into the mechanism, by demonstrating the following:

1. Activation of ARF1 mediates UPS of CFTR and SARS-CoV-2 Spike.
2. Activated ARF1 interacting with VAPA evokes UPS of CFTR by inducing autophagosome biogenesis in ER.

Furthermore, this study may also provide key information for novel therapeutic strategies for cystic fibrosis and COVID-19.

REFERENCES

1. Malhotra V. Unconventional protein secretion: an evolving mechanism. EMBO J 2013;32:1660-4.
2. Rabouille C. Pathways of Unconventional Protein Secretion. Trends Cell Biol 2017;27:230-40.
3. Gee HY, Noh SH, Tang BL, Kim KH, Lee MG. Rescue of DeltaF508-CFTR trafficking via a GRASP-dependent unconventional secretion pathway. Cell 2011;146:746-60.
4. Noh SH, Gee HY, Kim Y, Piao H, Kim J, Kang CM, et al. Specific autophagy and ESCRT components participate in the unconventional secretion of CFTR. Autophagy 2018;14:1761-78.
5. Park H, Shin DH, Sim JR, Aum S, Lee MG. IRE1alpha kinase-mediated unconventional protein secretion rescues misfolded CFTR and pendrin. Sci Adv 2020;6:eaax9914.
6. Lee MG, Ohana E, Park HW, Yang D, Muallem S. Molecular mechanism of pancreatic and salivary gland fluid and HCO3- secretion. Physiol Rev 2012;92:39-74.
7. Lukacs GL, Verkman AS. CFTR: folding, misfolding and correcting the DeltaF508 conformational defect. Trends Mol Med 2012;18:81-91.
8. Travers KJ, Patil CK, Wodicka L, Lockhart DJ, Weissman JS, Walter P. Functional and genomic analyses reveal an essential coordination between the unfolded protein response and ER-associated degradation. Cell 2000;101:249-58.
9. Watanabe Y, Allen JD, Wrapp D, McLellan JS, Crispin M. Site-specific glycan analysis of the SARS-CoV-2 spike. Science 2020;369:330-3.
10. Peacock TP, Goldhill DH, Zhou J, Baillon L, Frise R, Swann OC, et al. The furin cleavage site in the SARS-CoV-2 spike protein is required for transmission in ferrets. Nat Microbiol 2021;6:899-909.

11. Ujike M, Taguchi F. Incorporation of spike and membrane glycoproteins into coronavirus virions. Viruses 2015;7:1700-25.
12. YU X, Breitman M, Goldberg J. A Structure-Based Mechanism for Arf1-Dependent Recruitment of Coatomer to Membranes. Cell;148:530–42.
13. Dell'Angelica EC, Bonifacino JS. Coatopathies: Genetic Disorders of Protein Coats. Annu Rev Cell Dev Biol 2019;35:131-68.
14. Mesmin B, Bigay J, Moser von Filseck J, Lacas-Gervais S, Drin G, Antonny B. A four-step cycle driven by PI(4)P hydrolysis directs sterol/PI(4)P exchange by the ER-Golgi tether OSBP. Cell 2013;155:830-43.
15. Park H, Seo SK, Sim JR, Hwang SJ, Kim YJ, Shin DH, et al. TMED3 Complex Mediates ER Stress-Associated Secretion of CFTR, Pendrin, and SARS-CoV-2 Spike. Adv Sci (Weinh) 2022:e2105320.
16. Dascher C, Balch WE. Dominant inhibitory mutants of ARF1 block endoplasmic reticulum to Golgi transport and trigger disassembly of the Golgi apparatus. J Biol Chem 1994;269:1437-48.
17. Yoo JS, Moyer BD, Bannykh S, Yoo HM, Riordan JR, Balch WE. Non-conventional trafficking of the cystic fibrosis transmembrane conductance regulator through the early secretory pathway. J Biol Chem 2002;277:11401-9.
18. Chu DKW, Pan Y, Cheng SMS, Hui KPY, Krishnan P, Liu Y, et al. Molecular Diagnosis of a Novel Coronavirus (2019-nCoV) Causing an Outbreak of Pneumonia. Clin Chem 2020;66:549-55.
19. Russell C, Stagg SM. New insights into the structural mechanisms of the COPII coat. Traffic 2010;11:303-10.
20. Hong W. SNAREs and traffic. Biochim Biophys Acta 2005;1744:120-44.
21. TAKATSU H, YOSHINO K, TODA K, NAKAYAMA K. GGA proteins associate with Golgi membranes through interaction between their GGAH domains and ADP-ribosylation factors. Biochem. J. 2002;365:369–78.
22. Serafini T, Orci L, Amherdt M, Brunner M, Kahn RA, Rothmant JE. ADP-

Ribosylation Factor Is a Subunit of the Coat of Golgi-Derived COP-Coated Vesicles: A Novel Role for a GTP-Binding Protein

23. Ward CL, Omura S, Kopito RR. Degradation of CFTR by the ubiquitin-proteasome pathway. Cell 1995;83:121-7.
24. Zhao YG, Liu N, Miao G, Chen Y, Zhao H, Zhang H. The ER Contact Proteins VAPA/B Interact with Multiple Autophagy Proteins to Modulate Autophagosome Biogenesis. Curr Biol 2018;28:1234-45 e4.
25. Mizushima N, Yoshimori T. How to interpret LC3 immunoblotting. Autophagy 2007;3:542-5.
26. Saraste J, Prydz K. Assembly and Cellular Exit of Coronaviruses: Hijacking an Unconventional Secretory Pathway from the Pre-Golgi Intermediate Compartment via the Golgi Ribbon to the Extracellular Space. Cells 2021;10.
27. Minakshi R, Padhan K, Rani M, Khan N, Ahmad F, Jameel S. The SARS Coronavirus 3a protein causes endoplasmic reticulum stress and induces ligand-independent downregulation of the type 1 interferon receptor. PLoS One 2009;4:e8342.
28. Zhang J, Ejikemeuwa A, Gerzanich V, Nasr M, Tang Q, Simard JM, et al. Understanding the Role of SARS-CoV-2 ORF3a in Viral Pathogenesis and COVID-19. Front Microbiol 2022;13:854567.
29. Galluzzi L, Pietrocola F, Levine B, Kroemer G. Metabolic control of autophagy. Cell 2014;159:1263-76.
30. Rogov V, Dotsch V, Johansen T, Kirkin V. Interactions between autophagy receptors and ubiquitin-like proteins form the molecular basis for selective autophagy. Mol Cell 2014;53:167-78.
31. Jiang S, Dupont N, Castillo EF, Deretic V. Secretory versus degradative autophagy: unconventional secretion of inflammatory mediators. J Innate Immun 2013;5:471-9.
32. Ponpuak M, Mandell MA, Kimura T, Chauhan S, Cleyrat C, Deretic V. Secretory

autophagy. Curr Opin Cell Biol 2015;35:106-16.

33. Wijdeven RH, Janssen H, Nahidiazar L, Janssen L, Jalink K, Berlin I, et al. Cholesterol and ORP1L-mediated ER contact sites control autophagosome transport and fusion with the endocytic pathway. Nat Commun 2016;7:11808.
34. Tooze SA, Yoshimori T. The origin of the autophagosomal membrane. Nat Cell Biol 2010;12:831-5.
35. Nakatsu F, Kawasaki A. Functions of Oxysterol-Binding Proteins at Membrane Contact Sites and Their Control by Phosphoinositide Metabolism. Front Cell Dev Biol 2021;9:664788.
36. Chakraborty S, Doktorova M, Molugu TR, Heberle FA, Scott HL, Dzikovski B, et al. How cholesterol stiffens unsaturated lipid membranes. Proc Natl Acad Sci U S A 2020;117:21896-905.
37. Gomez RE, Chambaud C, Lupette J, Castets J, Pascal S, Brocard L, et al. Phosphatidylinositol-4-phosphate controls autophagosome formation in Arabidopsis thaliana. nature communications 2022.
38. Martens S, Nakamura S, Yoshimori T. Phospholipids in Autophagosome Formation and Fusion. J Mol Biol 2016.
39. Ilnytska O, Santiana M, Hsu NY, Du WL, Chen YH, Viktorova EG, et al. Enteroviruses harness the cellular endocytic machinery to remodel the host cell cholesterol landscape for effective viral replication. Cell Host Microbe 2013;14:281-93.
40. Zhang L, Hong Z, Lin W, Shao RX, Goto K, Hsu VW, et al. ARF1 and GBF1 generate a PI4P-enriched environment supportive of hepatitis C virus replication. PLoS One 2012;7:e32135.
41. Contreras I, Ortiz-Zapater E, Aniento F. Sorting signals in the cytosolic tail of membrane proteins involved in the interaction with plant ARF1 and coatomer. Plant J 2004;38:685-98.
42. Anwar MU, Sergeeva OA, Abrami L, Mesquita F, Lukonin I, Amen T, et al.

Anthrax intoxication reveals that ER-Golgi membrane contact sites control the formation of plasma membrane lipid nanodomain. 2022.

43. Skehel PA, Fabian-Fine R, Kandel ER. Mouse VAP33 is associated with the endoplasmic reticulum and microtubules. PNAS 2000;97:1101-6.
44. Wu H, Carvalho P, Voeltz GK. Here, there, and everywhere: The importance of ER membrane contact sites. Science 2018;361.
45. Soussan L, Burakov D, Mathew P, Daniels MP, Achituv MT, Porat A, et al. ERG30, a VAP-33–related Protein, Functions in Protein Transport Mediated by COPI Vesicles. The Journal of Cell Biology 1999;146:301-11.
46. Kanekura K, Nishimoto I, Aiso S, Matsuoka M. Characterization of amyotrophic lateral sclerosis-linked P56S mutation of vesicle-associated membrane protein-associated protein B (VAPB/ALS8). J Biol Chem 2006;281:30223-33.
47. Kanekura K, Suzuki H, Aiso S, Matsuoka M. ER stress and unfolded protein response in amyotrophic lateral sclerosis. Mol Neurobiol 2009;39:81-9.
48. Nthiga TM, Kumar Shrestha B, Sjottem E, Bruun JA, Bowitz Larsen K, Bhujabal Z, et al. CALCOCO1 acts with VAMP-associated proteins to mediate ER-phagy. EMBO J 2020;39:e103649.
49. Nishimura AL, Mitne-Neto M, Silva HC, Richieri-Costa A, Middleton S, Cascio D, et al. A mutation in the vesicle-trafficking protein VAPB causes late-onset spinal muscular atrophy and amyotrophic lateral sclerosis. Am J Hum Genet 2004;75:822-31.
50. James C, Kehlenbach RH. The Interactome of the VAP Family of Proteins: An Overview. Cells 2021;10.
51. Li J, Mahajan A, Tsai M. Ankyrin Repeat: A Unique Motif Mediating Protein−Protein Interactions. Biochemistry 2006;45:15168–78.
52. Johansson M, Lehto M, Tanhuanpaa K, Cover TL, Olkkonen VM. The oxysterol-binding protein homologue ORP1L interacts with Rab7 and alters functional properties of late endocytic compartments. Mol Biol Cell 2005;16:5480-92.

53. Lee JG, Takahama S, Zhang G, Tomarev SI, Ye Y. Unconventional secretion of misfolded proteins promotes adaptation to proteasome dysfunction in mammalian cells. Nat Cell Biol 2016;18:765-76.
54. Stark C, Breitkreutz BJ, Reguly T, Boucher L, Breitkreutz A, Tyers M. BioGRID: a general repository for interaction datasets. Nucleic Acids Res 2006;34:D535-9.
55. Ashour HM, Elkhatib WF, Rahman MM, Elshabrawy HA. Insights into the Recent 2019 Novel Coronavirus (SARS-CoV-2) in Light of Past Human Coronavirus Outbreaks. Pathogens 2020;9.
56. Perlman S, Netland J. Coronaviruses post-SARS: update on replication and pathogenesis. Nat Rev Microbiol 2009;7:439-50.
57. Lee JG, Huang W, Lee H, van de Leemput J, Kane MA, Han Z. Characterization of SARS-CoV-2 proteins reveals Orf6 pathogenicity, subcellular localization, host interactions and attenuation by Selinexor. Cell Biosci 2021;11:58.
58. Yun-Bin L, Minkyo J, Jeesoo K, Myeong-Gyun K, Chulhwan K, Jong-Seo K, et al. Endomembrane systems are reorganized by ORF3a and Membrane (M) of SARS-CoV-2. 2021.
59. Ritchie G, Harvey DJ, Feldmann F, Stroeher U, Feldmann H, Royle L, et al. Identification of N-linked carbohydrates from severe acute respiratory syndrome (SARS) spike glycoprotein. Virology 2010;399:257-69.
60. Grant OC, Montgomery D, Ito K, Woods RJ. Analysis of the SARS-CoV-2 spike protein glycan shield reveals implications for immune recognition. Sci Rep 2020;10:14991.
61. Tsai YL, Ha DP, Zhao H, Carlos AJ, Wei S, Pun TK, et al. Endoplasmic reticulum stress activates SRC, relocating chaperones to the cell surface where GRP78/CD109 blocks TGF-beta signaling. Proc Natl Acad Sci U S A 2018;115:E4245-E54.
62. D'Souza-Schorey C, Chavrier P. ARF proteins: roles in membrane traffic and beyond. Nat Rev Mol Cell Biol 2006;7:347-58.

63. Wang Q, He Z, Zhang J, Wang Y, Wang T, Tong S, et al. Overexpression of endoplasmic reticulum molecular chaperone GRP94 and GRP78 in human lung cancer tissues and its significance. Cancer Detect Prev 2005;29:544-51.
64. Kim KM, Yu TK, Chu HH, Park HS, Jang KY, Moon WS, et al. Expression of ER stress and autophagy-related molecules in human non-small cell lung cancer and premalignant lesions. Int J Cancer 2012;131:E362-70.
65. Van Krieken R, Tsai YL, Carlos AJ, Ha DP, Lee AS. ER residential chaperone GRP78 unconventionally relocalizes to the cell surface via endosomal transport. Cell Mol Life Sci 2021;78:5179-95.

ABSTRACT (IN KOREAN)

막 단백질의 비전형적 세포막 수송에서 ARF1의 역할

<지도교수 이민구>

연세대학교 대학원 의과학과

서 수 경

막 단백질이 소포체와 골지를 거치는 전형적 세포막 수송을 통해 세포막까지 도달하는 것은 굉장히 일반적인 이야기 이지만, 소포체 스트레스 상황에서 몇몇 막 단백질은 골지를 거치지 않는 비전형적 세포막 수송을 통해 세포막까지 이동이 가능하다. 그러나, 이러한 과정의 분자적 메커니즘은 아직 잘 알려진 바가 없다. 해당 연구는 ARF1의 활성화가 막 단백질의 비전형적 세포막 수송에서 필수적인 단계임을 확인하였다. ARF1의 여러 변이 중 활성화 상태로만 존재하는 변이는 비전형적 세포막 수송을 유도하여 CFTR과 온전한 Spike를 세포막에 도달시켰지만, 비활성화 상태로만 존재하는 변이는 그러지 못하였다. 또한, ARF1의 유전자 발현을 억제하면 CFTR과 Spike의 비전형적 세포막 수송이 감소하였다. 활성화된 ARF1은 ARF1-OSBPL1-VAPA 복합체를 형성하였고, 이는 CFTR 근처에서 비전형적 세포막 수송과 관련이 깊다고 알려진 자가포식소체의 형성을 유도하였다. 이러한 결과들은 ARF1이 골지를 우회하는 여러 막 단백질의 비전형적 세포막 수송에서 공통적 역할을 수행하고 있음을 시사한다.

핵심되는 말 : 비전형적 세포막 수송; 막 단백질; 세포 내 단백이동; 코로나바이러스; ARF1; VAPA; OSBPL1; CFTR; Spike;

PUBLICATION LIST

1. Park H*, **Seo SK***, Sim JR*, Hwang SJ*, Kim YJ*, Shin DH, et al. TMED3 Complex Mediates ER Stress-Associated Secretion of CFTR, Pendrin, and SARS-CoV-2 Spike. Adv Sci (Weinh) 2022:e2105320. (*equal contribution)